metals

Article

Tensile and Bending Behaviour of Steel–Glass Fibre-Reinforced and Non-Reinforced Steel–Polyamide Sandwich Materials

Wei Hua [1,*], Mohamed Harhash [1,2,3,*], Gerhard Ziegmann [2,4], Adele Carradò [5] and Heinz Palkowski [1,6,*]

1 Institute of Metallurgy, TU Clausthal, Robert-Koch-Straße 42, 38678 Clausthal-Zellerfeld, Germany
2 Clausthal Centre of Material Technology, TU Clausthal, Agricolastrasse 2, 38678 Clausthal-Zellerfeld, Germany; ziegmann@puk.tu-clausthal.de
3 Department of Metallurgical and Materials Engineering, Faculty of Petroleum and Mining Engineering, Suez University, Suez 43512, Egypt
4 Institute of Polymer Materials and Plastics Engineering, TU Clausthal, Agricolastrasse 6, 38678 Clausthal-Zellerfeld, Germany
5 Institute of Physics and Chemistry of Materials of Strasbourg, University of Strasbourg, 23 Rue du Loess, 67034 Strasbourg, France; carrado@unistra.fr
6 Space Engineering Department, Samara National Research University, Moskovskoye Hwy 34, 443086 Samara, Russia
* Correspondence: wei.hua@tu-clausthal.de (W.H.); mohamed.harhash@tu-clausthal.de (M.H.); heinz.palkowski@tu-clausthal.de (H.P.)

Abstract: The newly-developed thermoplastic-based fibre metal laminates (T-FML) show good prospects for their application in the automotive industry because of their lightweight potential and thermal formability. This paper focuses on describing the tensile and bending properties of this hybrid material as structural components for load-bearing parts in vehicles. For this purpose, the uniaxial tensile and four-point bending behaviours of steel/glass fibre-reinforced polyamide 6 (GF-PA6)/steel-laminates are investigated. The effects of cover/core layer thickness ratio and fibre weaving style on their tensile and bending properties are considered, while the span-to-thickness ratio was kept constant. Testing of the mono-materials and laminates of Metal/PA6/Metal (MPM) is performed to be considered as a reference. Further, the analytical method is validated to predict the bending properties of the laminates. A good agreement between the analytical values and experimental results regarding the bending strength and modulus is revealed. T-FML showed better tensile and bending properties with increasing fibre content compared to the GF-PA6 mono-organosheet and MPM.

Keywords: sandwich materials; thermoplastic-based fibre metal laminates; steel; polyamide 6; tensile and bending properties

Citation: Hua, W.; Harhash, M.; Ziegmann, G.; Carradò, A.; Palkowski, H. Tensile and Bending Behaviour of Steel–Glass Fibre-Reinforced and Non-Reinforced Steel–Polyamide Sandwich Materials. *Metals* **2023**, *13*, 1291. https://doi.org/10.3390/met13071291

Received: 31 May 2023
Revised: 6 July 2023
Accepted: 12 July 2023
Published: 18 July 2023

1. Introduction

1.1. Sandwich Materials

Sandwich materials have been developed for decades as 1/2 hybrid laminate systems offering lightweight potential and improved mechanical properties, e.g., the fibre metal laminates (FML) with advantages like low density, high strength, fatigue insensitivity, excellent resistance to damage, and high specific load-bearing capacity [1–4]. Different mono-material combinations and production processes are developed and designed to meet the desired structural and performance requirements of modern materials, such as the carbon fibre-reinforced polymer (CFRP), glass fibre-reinforced polymer (GFRP), Magnesium (Mg) alloy, Titanium (Ti) alloy, Aluminium (Al) alloy, etc. The first-developed FML was ARALL® (Aramid-fibre Reinforced Aluminium Laminates), which is thermoset-based and introduced to the market by Fokker as a wing structure in the Fokker F-27 Friendship [1]. Due to the disadvantages of Aramid fibres, such as low interfacial bond strength and insufficient fatigue resistance, improved products such as CARALL® (Carbon-fibre Reinforced Aluminium Laminates) and GLARE® (Glass-fibre Reinforced Aluminium

Laminates) continued to be developed and applied in, e.g., the A380 wing structure [5,6]. However, these thermoset-based FMLs exhibit low formability after curing of the resin matrix due to its plastic nature, which restricts their application in the automotive industry in terms of manufacturing cost. Currently, T-FML offers the possibility of mass production by using fibre-reinforced thermoplastics, such as the steel/GF-PA6/steel laminates developed in the LEIKA project, as they can be formed into complex shapes at elevated temperatures, keeping in mind the possible processing challenges [7]. Similar hybrid systems of CAPET® (Titanium(Ti)/Carbon fibre-reinforced polyetheretherketone/Titanium) and CAPAAL® (Al/Carbon fibre-reinforced polyamide/Al) have also been developed due to the excellent lightweight properties and mechanical properties of Ti-alloys, Al-alloys, and carbon fibres [8–10]. The approach to developing thermoplastic-based FML is promising and novel; however, several aspects have to be overcome and understood, e.g., forming, interface properties, failure, modelling, and simulation. Another sandwich type, MPM laminates with non-reinforced cores, are not as robust and stiff as FML, but they also have lightweight properties and gain future benefits in terms of weight saving and reduction of CO_2 emissions and fuel consumption in the automotive sector. Litecor, for example, developed by thyssenkrupp Steel Europe, is ideally suited to the lightweight construction of flat components in vehicle construction, such as roofs, doors, tailgates, and bonnets, as well as interior components such as parcel shelves or vehicle floors [11]. Further products are available such as Hylite® (Al/polypropylene/Al), Dibond® and Alucobond® (Al/polyethylene/Al), Steelite® (steel/polypropylene/steel) and Usilight® (steel/polypropylene or polyethylene/steel) [6].

1.2. Tensile and Bending Behaviour of Sandwich Materials

Sandwich materials are usually used as a panel structure in automotive or aircraft manufacturing, in which the tensile and bending properties are the main two factors influencing their structural performance. They depend on the integral strength of the sandwich materials, which is determined by the respective properties of the core (pure polymer or composite) and metallic cover layers and the strength of their interfacial adhesion. The tensile strength of the sandwich material with or without fibre reinforcement can be prior estimated by obeying the rule of mixture (ROM), describing a weighted mean to predict various properties of a composite material [12]. A key factor affecting the integral tensile strength of the sandwich material is the core layer, the properties of which depend on the fibre content, fibre orientation, adhesion strength with covers, etc. [13]. For example, the tensile strength of FMLs is obviously higher than those with pure plastic cores [14]. And the tensile and impact strength of the unidirectional composite is higher than the twill-woven composite, which is more beneficial for load-bearing members in the automotive sector [15]. But it faces the challenge of being highly anisotropic, with high stiffness and strength values in the longitudinal fibre direction and poor mechanical properties in the transverse direction [16]. However, it seems difficult to predict the bending properties of the sandwich materials, which also depends on the material combinations. Furthermore, based on the current literature survey, no empirical methods like ROM have been found to calculate their bending strength or modulus, nor has the relationship between tensile and bending properties been described. One of our previous works has revealed that the three-dimensional T-FML structures gain good impact resistance, reported in [12], in which the T-FMLs composed of Steel/Twill-GF-PA6/Steel and Al/Twill-GF-PA6/Al are produced into single-hat-profiles through the novel one-step thermoforming process. For tailored designing of FML structures with good structural performance, predicting their tensile and bending properties through empirical methods or describing their relationship seems more efficient. Furthermore, the factors influencing their mechanical properties need to be characterized as well.

Commonly used methods to characterize these properties are the uniaxial tensile test and the three- or four-point bending tests [17,18]. The four-point bending method has a clear advantage over the three-point bending method because it offers better load distribution and avoids strong local damage under loading rollers [19]. The choice of the sample size and the test setup is therefore the major concern for the bending tests. Currently, there is no standard for conducting four-point bending tests on sandwich materials. For example, for test setup, the span-to-thickness ratio gains more attention, as it affects the bending properties significantly. The smaller the span-to-thickness ratio of the FML sample, the earlier the failure during the bending test [20], as the interlaminar shear strength is significantly lower compared to the in-plane shear strength at the small span lengths. The sandwich samples are subjected to higher interlaminar shear stresses relative to the bending stresses, resulting in delamination between their layers. In this respect, the shear damage mode dominates, resulting in an overestimation of the bending strength determined analytically or numerically, particularly for the FML samples. Therefore, large span-to-thickness ratios are recommended for four-point bending tests. For example, span-to-thickness ratios for unidirectional and cross-ply laminates range from 14 to 24 and 15 to 27, respectively [21].

1.3. Aim and Structure of the Paper

In the last decade, the T-FMLs composed of steel covers and a thermoplastic core (GF-PA6) or similar material combinations have gained increasing attention in the automotive industry; their panel structure manufactured via the novel one-step thermal forming method indicts good impact strength, as mentioned in [12]. The influencing factors that affect the bending and tensile properties of these FMLs need further investigation. For the tailored design of an FML structure like the top-hat profile in [12], basic analysis is still needed. Despite the analytical analysis, some experimental characterization of the following material combination will be conducted:

- Sandwich material with a glass–fibre reinforced polyamide 6 core, i.e., steel/GF-PA6/steel;
- Sandwich material with non-reinforced polyamide 6 core, i.e., steel/PA6/steel.

For analytical calculation, material characterization via tensile tests is needed to characterize.

For this purpose, a systematic investigation starting with mono-materials and MPM as a reference followed by FML is carried out. This paper is structured as follows. The materials used and sandwich production process are first described in Section 2.1, while the test procedure including the bending tool design and the experimental plan are described in Section 2.2, followed by the description of the analytical method in Section 2.3. The discussion of the tensile and bending results is given in Sections 3.1 and 3.2. At the end, the validation of the analytical calculation is given in Section 3.3. A summary will be presented in Section 4.

2. Experimental and Analytical Work

2.1. Materials

In this study, the electro-galvanised steel grade TS275 (grade 1.0375, thickness 0.4 mm) from thyssenkrupp Steel Europe, an unalloyed low-carbon steel used mainly in the food packaging industry and more recently in the automotive industry, was used because of its thin thickness, good ductility, and moderate strength. The thermoplastic core is made of PA6 film (0.5 mm) supplied by Infiana Germany GmbH & Co. KG (Forchheim, Germany). The different PA6 core thicknesses are achieved by laminating and thermal fusing multi-PA6 films, which have a melting point of 220 °C. The used mono-materials are summarized in Table 1. The reinforced organosheets are GF-PA6 from Lanxess with a fibre volume fraction of 47% and are available in 0.5, 1.0, and 2.0 mm thicknesses. Two kinds of organosheets are chosen, namely:

- Tepex RG with a twill 2/2 weaving style, 50% of fibres in each weft and warp directions;
- Tepex RGUD with a unidirectional weaving style, 20% of fibres in weft and 80% in warp directions, accompanied by less fibre undulation compared to RG.

Table 1. Summary of the used materials.

Materials/ Abbreviation	Thickness [mm]	Coating	Fibre Content [vol.-%]	Supplier
TS275	0.4	Zinc	–	thyssenkrupp Steel Europe AG (Kaiser-Wilhelm-Strasse, Duisburg, Germany)
PA6	0.5	–	–	Infiana Germany GmbH & Co. KG (Forchheim, Germany)
RG	0.5, 1.0, 2.0	–	47	Lanxess Deutschland GmbH (International Business Park, Singapore)

In order to investigate the tensile and bending behaviours of the sandwich materials, the semi-finished sandwich panels are first prepared. In this respect, the mono-materials need to be pre-treated before they are subjected to hot-pressing for the production of the sandwich panels. On the one hand, the core material is simply cleaned with acetone and then dried at 80 °C for at least 12 h to ensure that the moisture content in the matrix PA6 is as low as possible. The steel sheets, on the other hand, are cleaned, ground (grid size 60: abbreviated as G_60), tempered (1 min at 440 °C: abbreviated as HT_440 °C/1 min), and then spread with the adhesion promoter SI-Coating, which is activated at 250 °C for 3 min. This preparation scenario is recommended based on a previous study [22]. After completing the pre-treatment of the individual materials, they are stacked together in the form of 2/1 and fed into a hot press with manufacturing conditions of 245 °C, 3 bar, and 5 min. Under these conditions, sufficient bond strength can be achieved, i.e., lap shear strength values of 20 to 25 MPa for MPM panels and approx. 16 MPa for FML panels [23]. The entire production process is shown schematically in Figure 1. After cooling under pressure for 5 min and undergoing consolidation, the sandwich panels were demoulded at approx. 80 °C. The samples for tensile and bending tests were obtained via a punching and cutting process from the square sandwich panel with a dimension of 200 × 200 mm^2. Further details regarding the surface preparation and sandwich production can be found in [23,24].

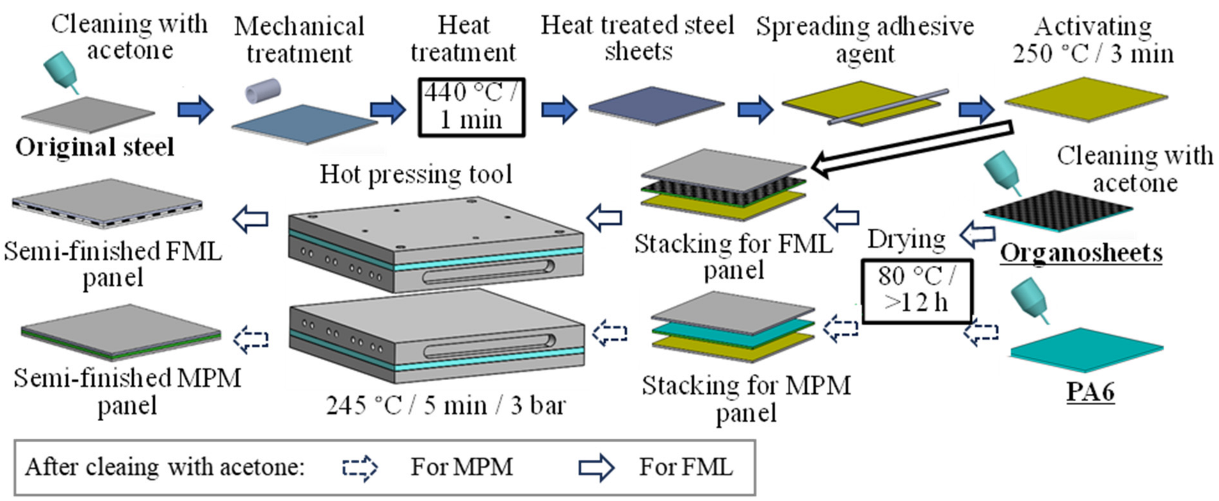

Figure 1. Surface treatments of cover and core layers and the production of sandwich panels by means of hot pressing.

2.2. Testing Procedure

The tensile mechanical properties were determined by performing tensile tests at a constant strain rate of 0.008 s^{-1} on the samples shown in Figure 2 according to DIN 50,125 [25]. The strain changes in the tensile test samples are monitored from one side using the digital image correlation (DIC) system. The aim of the tensile test procedure is to determine overall tensile properties such as yield strength, ultimate tensile strength, elastic modulus, strain hardening index, anisotropy, and elongation at failure.

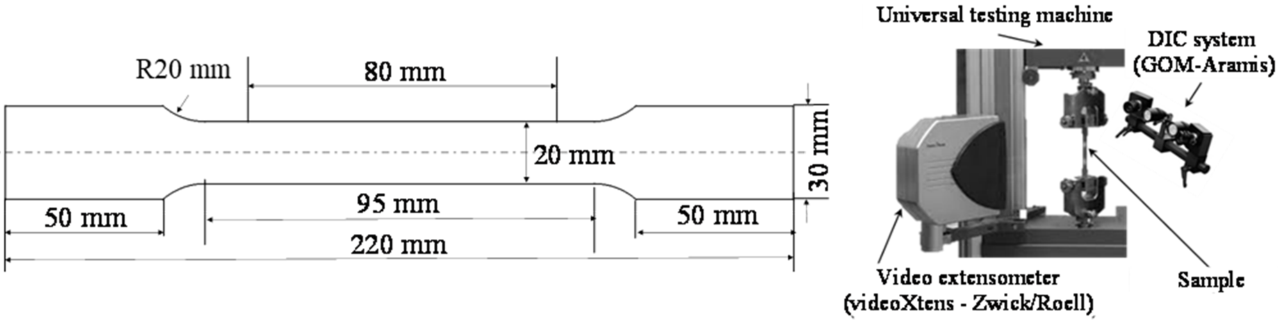

Figure 2. Sample geometry for the tensile test and the DIC unit.

According to DIN 14125, a four-point bending test is carried out on the sample according to the setup shown in Figure 3, describing the relationship between the span, sample length, and thickness. In addition, the radii of the press fins and the support rollers are kept at 2 mm when the total thickness of the sample is less than 3 mm. The test speed is 2 mm/s. The dimensions of the samples, as well as the span width, are shown in Figure 3.

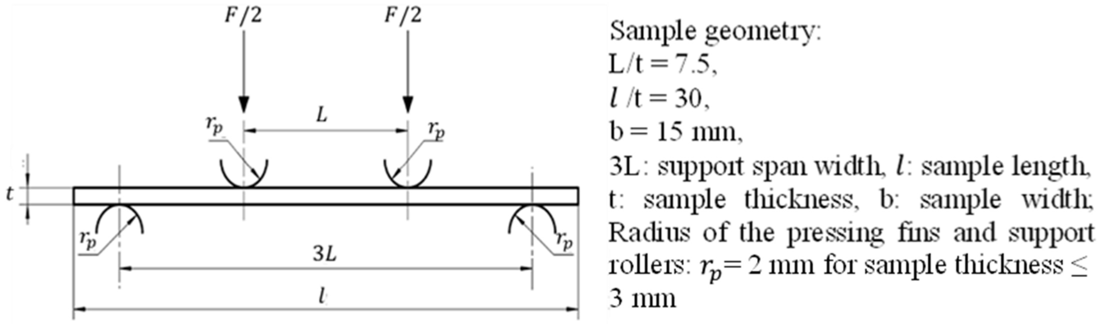

Figure 3. Test setup for four-point bending according to DIN 14125.

Furthermore, in order to clearly identify each material combination in the following diagram, it is necessary to abbreviate the sandwich materials as shown in Table 2 for the different sandwich panels. In this respect, MPM and FML panels with different core layer thicknesses were tested, as well as organosheets RG and RGUD with a thickness of 1.0 mm. The test conditions are given in Table 3.

Table 2. Abbreviation of sandwich panels.

Abbreviation	Sandwich Panels
MPM-PAx	MPM based on TS275/PA6/TS275 with core layer thickness x
FML-RGx	FML based on TS275/RG/TS275 with core layer thickness x
FML-RGUD^{X}x	FML based on TS275/RGUD/TS275 with core layer thickness x, ^{X}: warp direction of RGUD in sample length direction
FML-RGUD^{Y}x	FML based on TS275/RGUD/TS275 with core layer thickness x, ^{Y}: weft direction of RGUD in sample length direction

The bending apparatus is shown in Figure 4, in which the press fins have an inclined angle of 45° so that the angle between the outer bevels of the two fins is 90°, marked with yellow lines in Figure 4. The bending test is stopped experimentally when the sample is punched to the end with the supports, indicated by an instantaneous increase in the bending force. At that time, two sides of the sample are clamped by the fins and rollers with the angle considered to be 90°. The corresponding experimental plan for the different tested materials is shown in Table 4. It describes the tensile and bending test series including the mono-materials and the sandwich materials composed of them. For the performed test regarding different material combinations and test types, the chosen thickness and test are noted with "x".

Table 3. The dimensions of the sample in 4-point-bending.

	Length *l* [mm]	Width *b* [mm]	Thickness *t* [mm]	Support Span 3*L* [mm]	Inner Fins Span *L* [mm]
RG/RGUD1.0	30	15	1.0	23	8
MPM-PA0.1	27	15	0.9	20	7
MPM-PA0.5	39	15	1.3	30	10
MPM-PA1.0	54	15	1.8	41	14
MPM-PA1.5	69	15	2.3	52	17.5
FML-RG0.5	39	15	1.3	30	10
FML-RG1.0	54	15	1.8	41	14
FML-RG2.0	84	15	2.8	63	21
FML-RGUD^{X}1.0	54	15	1.8	41	14
FML-RGUD^{Y}1.0	54	15	1.8	41	14

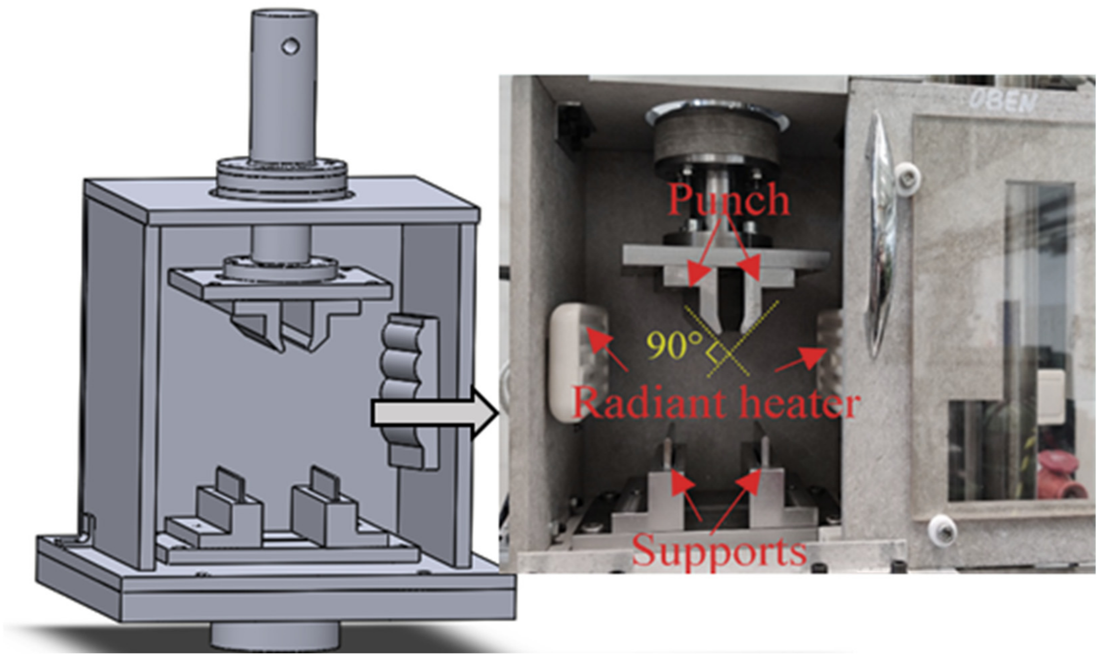

Figure 4. Tool design for four-point bending tests.

Table 4. Test plan for tensile test and four-point bending (with four repetitions each).

Material/ Abbreviation	Cover Sheet	Core Layer									Test	
	TS275 [mm]	PA6 [mm]				RG [mm]			RGUD [mm]		Tensile Test	4P-Bending
	0.4	0.1	0.5	1.0	1.5	0.5	1.0	2.0	0.5	1.0		
TS275	x										x	
PA6			x								x	
RG						x					x	
							x				x	x

Table 4. *Cont.*

Material/ Abbreviation	Cover Sheet	Core Layer									Test	
	TS275 [mm]	PA6 [mm]				RG [mm]			RGUD [mm]		Tensile Test	4P-Bending
	0.4	0.1	0.5	1.0	1.5	0.5	1.0	2.0	0.5	1.0		
RGUD									x		x	
										x		x
MPM	x	x										x
	x		x								x	x
	x			x							x	x
	x				x							x
FML	x					x					x	x
	x						x				x	x
	x							x				x
	x								x		x	
	x									x	x	x

x: performed.

After obtaining the force-displacement curves, the individual bending properties such as bending strength σ_b, bending modulus E_b, and interlaminar shear strength τ_{max} of the samples can be determined. If the sample fails or plastically yields, the maximum bending stress is defined as the bending strength σ_b. The following equations are used to calculate the bending stress σ_b and the bending modulus E_b according to DIN14125 [26].

$$\sigma_b = \frac{3FL}{bt^2} \tag{1}$$

$$E_b = \frac{0.21(3L)^3}{bt^3}\left(\frac{\Delta F}{\Delta s}\right) \tag{2}$$

where F is the maximum loading force, ΔF is the difference of the bending force in elastic range, and Δs is the difference of the bending depth in the elastic range.

If the delamination failure mode dominates in the bent sample, the interlaminar shear strength τ_{max} can be calculated according to Equation (3) [27].

$$\tau_{max} = \frac{3F}{4bt} \tag{3}$$

In addition to the above-mentioned bending properties, the strain evolution and failure modes of the bent samples—such as delamination and thickness irregularities—will be investigated by optical microscopy.

2.3. Analytic Analysis of the Four-Point-Bending Configuration

Moreover, it is of interest to introduce analytical methods to predict the bending behaviour in terms of the force evolution for bending sandwich samples in different compositions, sizes, and thicknesses directly. The analytical method could predict the force evolution of the bent sample under four-point bending conditions according to DIN 14125, as shown in Figure 5, assuming that the sandwich materials of MPM and FML are homogeneous materials and the equation terms regarding their mechanical properties are calculated according to the rules of mixing (ROM) for the laminates [28], as no specific standard is given to characterize the bending behaviour for FML or MPM [26]. In order to achieve a certain bending angle, the deflection of the punch "s" must be determined. s can be expressed in terms of the bending angle α according to Equation (4).

$$s = \left(2r_p + t\right)\left(1 - \frac{1}{\cos\alpha_x}\right) + \tan\alpha_x \cdot L \tag{4}$$

where $3L$ is the support span of the pressing fins, which depends on the sample thickness. Moreover, r_p is the bending radius of the pressing fin and support rollers, which is kept at 2.0 mm for sample thicknesses up to 3.0 mm. t is the total thickness of the bent sample and α is the bending angle. The bending force is calculated according to Equation (5) [29]:

$$F = \frac{2b\left\{C_1 cos^2\alpha_x + \left(\frac{C_2+C_4}{C_3}\right)\left[L\sin\alpha_x - \left(2r_p+t\right)\right]\right\}}{L-\left(2r_p+t\right)\sin\alpha_x} + \frac{2bC_1\mu(\alpha_x+\sin\alpha_x\cos\alpha_x)}{L-\left(2r_p+t\right)\sin\alpha_x} + \frac{2b\left\{\left(\frac{C_2+C_4}{C_3}\right)\mu\left[L\frac{\left(1+sin^2\alpha_x\right)}{\cos\alpha_x} - 2\left(2r_p+t\right)\tan\alpha_x\right]\right\}}{L-\left(2r_p+t\right)\sin\alpha_x} \tag{5}$$

where b is the sample width and m, C_1, C_2, C_3, and C_4 are material parameters. The derivation of these parameters is shown in Equations (6)–(10) [29]:

$$C_1 = \frac{\sigma_0 t^2}{4}\left[1 - \frac{m}{E} + \frac{mt}{6\sigma_0\left(r_p + \frac{t}{2}\right)}\right] \tag{6}$$

$$w = \frac{\sigma_0}{E}\left(r_p + \frac{t}{2}\right) \tag{7}$$

$$C_2 = \frac{2}{3}\frac{{\sigma_0}^3 t^2}{E}\left[\frac{\left(1-\frac{m}{E}\right)\left(\frac{t}{2}-w\right)}{4} + \frac{mt}{24E}\ln\left(\frac{t}{2w}\right) - \frac{2}{9}\frac{\left(1-\frac{m}{E}\right)}{t^2}\left(\frac{t^3}{8} - w^3\right)\right] \tag{8}$$

$$C_3 = \sigma_0\left(1 - \frac{m}{E}\right)\left[\frac{t^2}{4} - \frac{{\sigma_0}^2}{3E^2}\left(r_p + \frac{t}{2}\right)\right] \tag{9}$$

$$C_4 = \frac{{\sigma_0}^3 t^3}{108E} \tag{10}$$

$$m = \frac{\sigma_{pl} - \sigma_0}{\varepsilon_{pl} - \varepsilon_0} \quad \left(\sigma_0 \le \sigma_{pl} \le UTS\right) \tag{11}$$

where UTS is the ultimate tensile strength; σ_0, σ_{pl} are the yield and plastic strength, ε_0, ε_{pl} are the yield and plastic strain, respectively, and E is the elastic modulus.

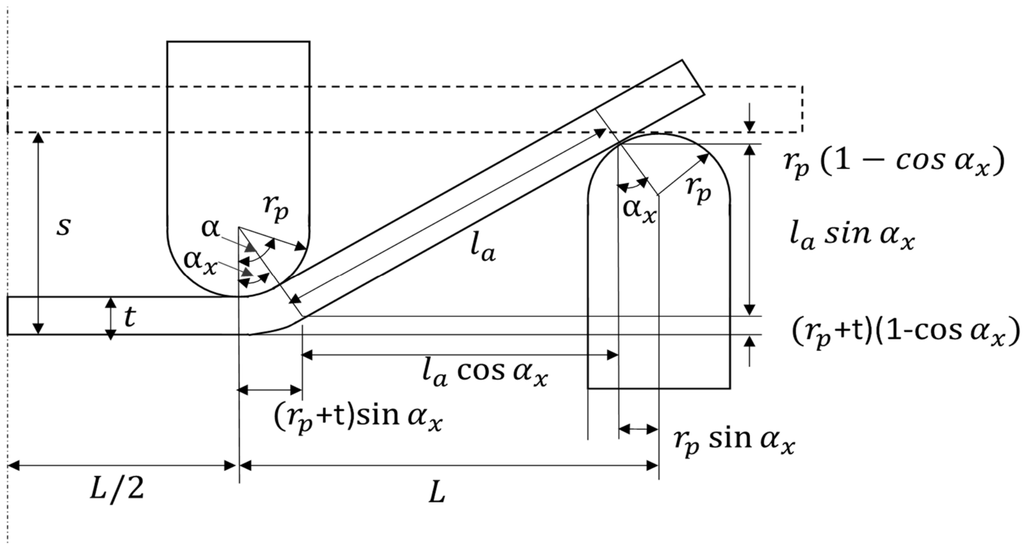

Figure 5. Geometrical schematic used for the force analysis under four-point bending conditions [29].

3. Results and Discussion

3.1. Tensile Test Results

As can be seen in Figure 6a, the tensile stresses of the monolithic steel sheet TS275 and the MPM composed of TS275 and PA6 are presented, in which the strength of MPM decreases with increasing core layer thickness, which is due to the absolute less strength of the PA6 core compared to the steel cover sheet. According to the rule of mixing (ROM) for sandwich materials, their overall strength decreases as the volume fraction of the core layer increases; the experimentally measured values are summarized in Table 5 together with the tensile strength and elastic modulus values estimated based on ROM. For the monolithic organosheets illustrated in Figure 6b, both the UTS and the elastic modulus increase gradually as the volume fraction of the fibres in the sample length direction increases, due to the fact that the strength of the fibres is higher than that of the matrix PA6. In addition, RG and $RGUD^X$ essentially showed a linear increase in their elastic deformation range, fracturing at the highest point with negligible plastic deformation. In contrast, the tensile stress of $RGUD^Y$ showed a concave linear trend with a decreasing slope of the curve as the strain increased. Both the tensile strength and elongation at failure were lower than RG and $RGUD^X$. The tensile strength is dependent on the fibre content in loading direction, which is lower for $RGUD^Y$ as expected. The lower failure strain is due to the easier stress and strain concentrations in the matrix between the fibres, resulting in an earlier formation of micro-cracks located at or near the fibre/matrix interface. It was reported that the transverse failure strain for the unidirectional composite is considerably lower than the longitudinal failure strain and decreases as fibre content increases in longitudinal directions [16]. The monolithic PA6, alternatively, has significantly less tensile strength and greater elongation at failure compared to the organosheets, which is due to its plastic nature.

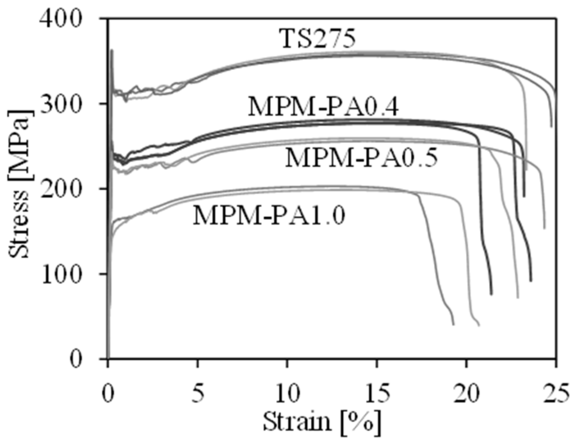

(**a**)

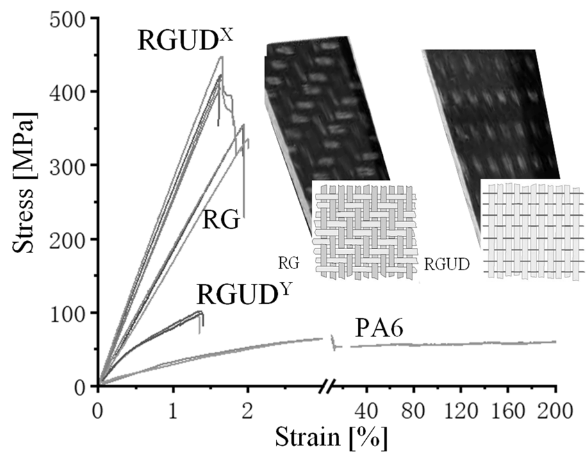

(**b**)

Figure 6. Tensile properties of (**a**) TS275 and MPM and (**b**) of PA6 and organosheets RG and RGUD as a benchmark.

Figure 7a depicts the tensile test results of FML with different organosheets. It can be seen that, the elastic modulus and yield strength of FML-RG and FML-$RGUD^X$/-$RGUD^Y$ do not differ from each other significantly. The main difference is observed in UTS, which increases significantly with the increasing fibre volume fraction in the tension direction. Moreover, the steel cover sheet provides backing support for the core organosheets RG and RGUD, showing a higher elongation at failure in the FML than the monolithic ones; a similar effect was reported in [30]. In Figure 7b, a comparison of FML-RG and FML-$RGUD^X$ for two core thicknesses is depicted. It can be seen that the yield strength of the FML becomes smaller as the core thickness increases and the UTS increases slightly. The tensile stress of organosheets is much smaller than the yield strength of the steel cover sheet at the yield point (Strain = 0.2%), in which the organosheets remain elastic until the fibre fracture at the end (Strain $\geq$ 2%).

Table 5. Summary of tensile test results and values calculated according to the ROM.

Material	*E* [GPa]	E^* [GPa]	*UTS* [MPa]	UTS^* [MPa]	*YS* [MPa]	e_f [%]
TS275	204 ± 2	—	363 ± 3	—	317 ± 4	24.5 ± 0.5
PA6	3 ± 0	—	73 ± 3	—	31 ± 8	–
RG	18 ± 1	—	338 ± 22	—	318 ± 9	1.9 ± 0.1
$RGUD^X$	30 ± 1	—	439 ± 25	—	382 ± 35	1.7 ± 0.1
$RGUD^Y$	14 ± 1	—	102 ± 8	—	60 ± 6	1.4 ± 0.1
MPM-PA0.4	145 ± 7	137	278 ± 2	266	239 ± 3	23 ± 1
MPM-PA0.5	131 ± 8	127	258 ± 14	247	225 ± 13	23.5 ± 1
MPM-PA1.0	96 ± 11	94	201 ± 3	199	155 ± 10	20 ± 1
FML-RG0.5	132 ± 6	136	400 ± 7	353	233 ± 2	—
FML-RG1.0	113 ± 5	103	425 ± 5	349	202 ± 3	—
FML-$RGUD^X$0.5	140 ± 6	140	450 ± 1	392	252 ± 1	—
FML-$RGUD^X$1.0	113 ± 3	110	468 ± 22	405	209 ± 5	—
FML-$RGUD^Y$0.5	130 ± 17	134	301 ± 3	263	231 ± 6	—

*: refers to the values estimated by the rule of mixtures (ROM).

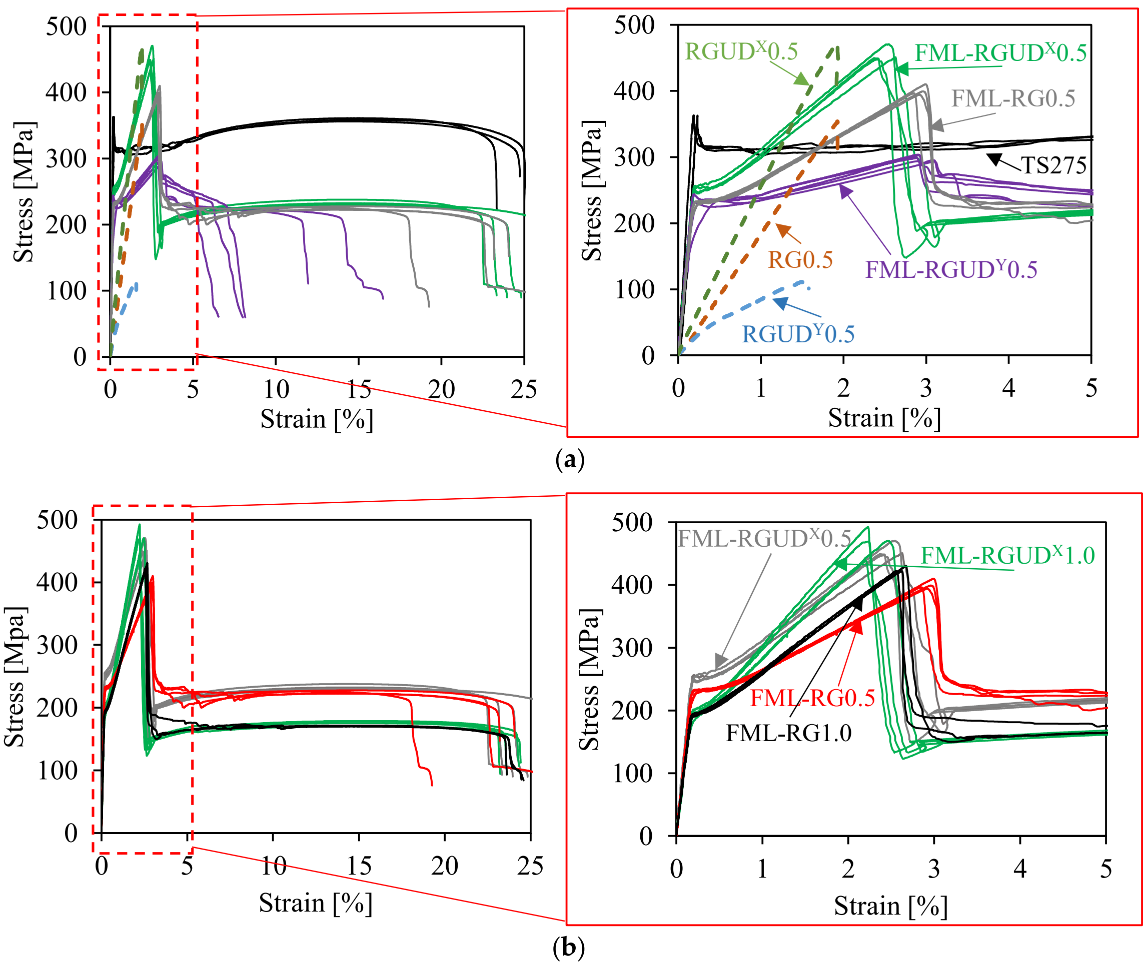

Figure 7. Tensile properties of (**a**) of FML with different organosheets and (**b**) of FML with different core thicknesses.

Furthermore, the typical failure mode of FMLs is depicted. After the elastic deformation stage, the metal layer begins to yield while the composite core layer remains elastic due to its linear elastic nature, so the bending force displacement curve generally shows two rising intervals, the latter possessing a smaller slope compared to the prior. At the end of the second stage of deformation, the monofilaments in the core begin to break and gradually form microcracks, where the normal stresses reach their maximum. After the peak force has been reached, the laminate begins to fail, with localized fracture of the composite core layer near the outer side and delamination from the metal cover layers. Similar results have been reported in [31,32], focusing on the inversely layered metal/FRP members like CFRP/Al/CFRP or multi-layered $\frac{3}{4}$ and 7/8-FMLs.

In Figure 8, the tensile sample images are illustrated. It can be seen that the fibre fracture of RG, RGUD^X, and RGUD^Y varies considerably. In RGUD^Y, fracture takes place neatly due to the lower fibre content in the tension direction, therewith more stress and strain concentration in the matrix and near matrix/fibre interface area, leading to early fracture. TS275 and MPM-PA0.5 have similar elongations at break and the bond between TS275 and PA6 is strong during tension, so no delamination occurs before the cover fractures. However, it is evident that both FML-RG and FML-RGUD^X delaminated after the organosheet core broke, whereas FML-RGUD^Y did not, with the red rectangle in the figure marking debonding and the green rectangle marking remaining bonding. This may be due to the higher interlaminar shear stress between the cover and the core layer after the organosheet fracture, while the interlaminar shear stress appears to be lower in FML-RGUD^Y, as the organosheet fractures earlier and the steel sheet undergoes stress concentration resulting in local plastic deformation. This phenomenon occurs frequently in FML-RGUD^Y, as shown in the forward force-displacement curves in Figure 7a.

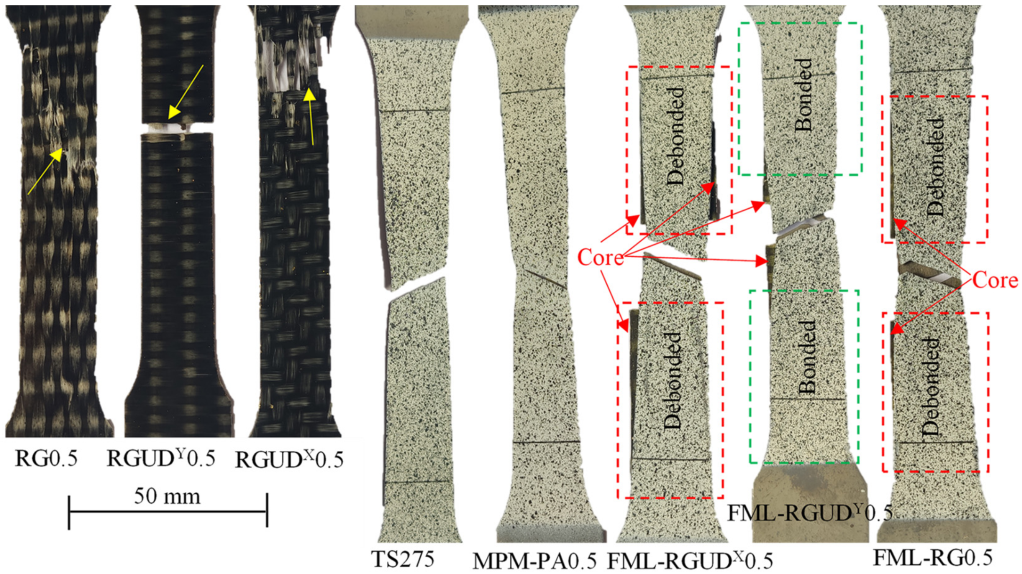

Figure 8. Tensile sample images.

In Figure 9, the DIC images of TS275, RG, MPM, FML-RG, and FML-RGUD for different strain values are illustrated. Firstly, in Figure 9a, the comparison between TS275, RG, and FML-RG0.5 is illustrated and has been published previously [12]. It can be seen that the Lüders bands appeared in TS275 at strain values of 0.5%, while the monolithic RG shows a strain extension in the 45° direction. At a strain value of 2.0%, the steel sheet continues to deform plastically with the extension of the Lüders bands, while damage is already present in the monolithic RG, marked by the red arrow. In contrast, the FML shows damage in the core RG at a strain value of 2.9%. The steel sheet continued to be tensioned after the core RG fractured, with the fracture occurring at 26% of the strain value, close to that of the monolithic TS275 [12]. In Figure 9b, the DIC images for the samples of MPM and FML-RGUD^X/-RGUD^Y are depicted. MPM shows the Lüders bands as the monolithic steel sheet, indicating the influence of core PA6 on the plastic deformation of the cover sheet TS275 is neglectable compared to the organosheet core in the FML-RG. In contrast, the FML-RGUD^{X}0.5 showed similar strain evolution to the FML-RG0.5, except for the earlier fracture of RGUD^X, marked by the red arrow in Figure 9b. Alternatively, the

FML-RGUD^{Y}0.5 showed more pronounced strain evolution in the perpendicular direction to the sample length before the fracture occurred in the sample middle (marked by the red arrow). This is due to the higher transverse normal strain in RGUD^Y in comparison to RGUD^X or RG [33,34]. As mentioned earlier, the plastic deformation of the cover in the FML-RGUD^Y is localised and therefore the total elongation of the cover is lower than the previous FML-RG and FML-RGUD^X, see Figure 9b, with an elongation of only 16% for the FML-RGUD^Y compared to 26% for the monolithic steel sheet.

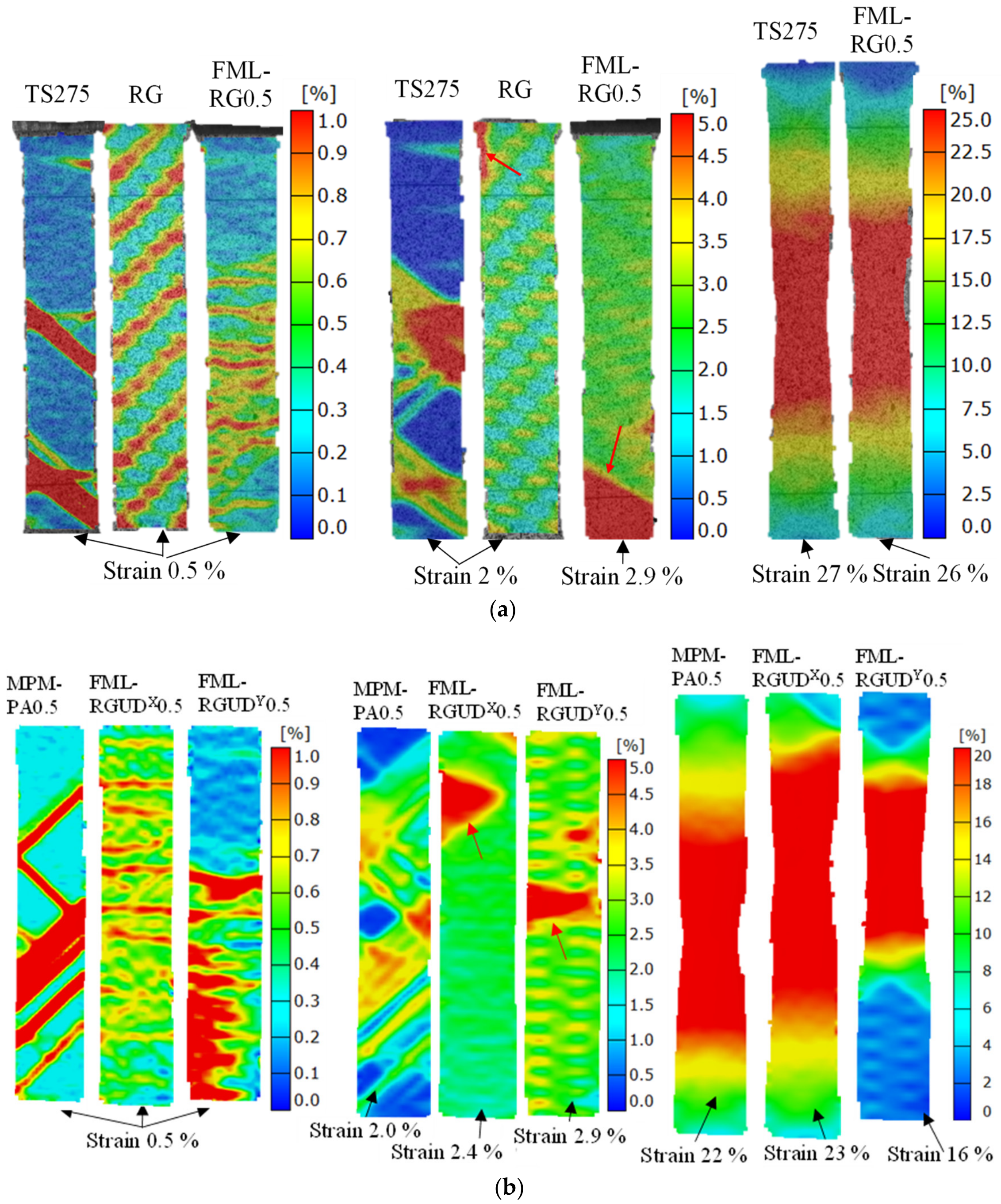

Figure 9. DIC-images of (**a**) TS275, RG, FML-RG0.5 [12] and (**b**) MPM-PA0.5, FML-RGUD^{X}0.5, FML-RGUD^{Y}0.5.

The tensile test results for E-modulus, YS, UTS, and elongation at failure for each mono-material and laminate are presented in Table 5. In addition, E^* and UTS^* are calculated based on ROM. It can be seen that the calculated values for E-modulus match very well with the experimental values for the MPM and FML. Furthermore, the calculated UTS values of MPM match well with the experimental values, but this is not the case for FML, which is due to the backing support of covers on the organosheets RG and RGUD in the FML, resulting in UTS being greater than the values calculated based on ROM.

3.2. Bending Results

3.2.1. Bending of the Organosheets

Figure 10a illustrates the bending strength σ_b and bending modulus E_b of the organosheets with different fibre orientations, in which both of them increase with the increasing volume fraction of fibres in the longitudinal direction of the sample, as expected. For instance, the bending strengths for RGUD^{Y}1.0, RG1.0, and RGUD^{X}1.0 are (257 ± 26) MPa, (561 ± 17) MPa, and (675 ± 30) MPa, respectively; and the bending moduli are (10.5 ± 3.7) GPa, (21.5 ± 1.7) GPa, and (23.8 ± 1.2) GPa, respectively. The measured bending strength and bending modulus of RG1.0 matches well with the supplier's technical data sheet [35], which are 580 MPa and 20 GPa. In addition, both RG and RGUD^{X} samples exhibited tensile failure at RT, while the failure mode of RGUD^{Y} was not recognisable, as shown in Figure 10b. The black and white stochastic patterns on the sample surface are sprayed for the DIC analysis.

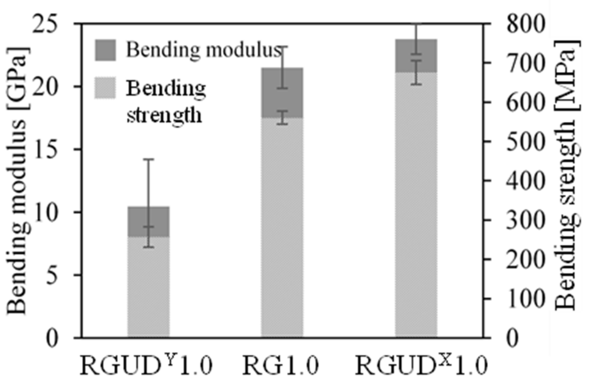

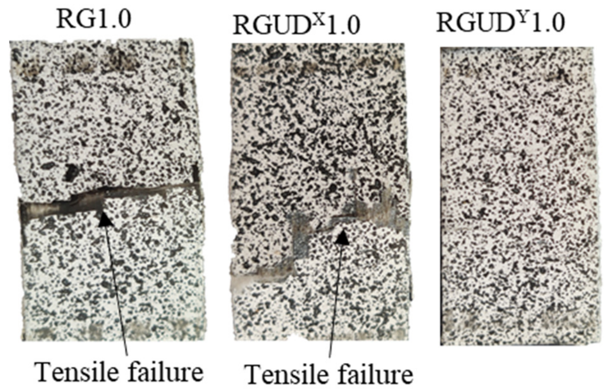

Figure 10. Results of (**a**) σ_b and E_b for organosheets RG and RGUD at RT and (**b**) fractures images for organosheets RG and RGUD.

3.2.2. Bending of the MPM

At RT, the bending forces for MPM increase slightly with increasing core layer thickness. All samples of MPM showed no failure, neither cracking nor delamination, after four-point bending, but only plastic deformation. The maximum bending stress (i.e., σ_b) and modulus of MPM were calculated and compared with experimental values. Both of them decreased with increasing the core thickness at RT. This is due to the lower bending strength and modulus of the monolithic PA6. As reported, the bending strength and modulus of monolithic PA6 is approx. 84 MPa and 2.3 GPa [36,37], which is significantly less than that of the steel sheet TS275. A linear relationship between the maximum bending stress and modulus of MPM and the core thickness at RT was found, as can be seen in Figure 11. From the inverse derivation of the empirical equation in Figure 11, assuming that the y value obtained when $x = 0$ is the bending strength and modulus of the monolithic steel sheet TS275 under four-point bending in this study, their values can be estimated to be (594 ± 10) MPa and (133 ± 10) GPa, respectively. All results obtained by testing MPM are used as a reference to highlight the differences for the FML in the next section. In addition, the measured bending strengths and moduli are compared with the tensile strength $UTS - ROM$ and elastic modulus $E - ROM$ (estimated based on ROM) in Figure 11. As the deviation between the experimental results and the ROM-based values is ignorable for MPM, the experimental values were not illustrated in the same figure. It can be seen that the bending modulus E_b is smaller than the elastic modulus $E - ROM$, in which the bending/elastic modulus ratio ranges from 0.7 to 0.8. The calculated bending modulus is mainly influenced by the chosen span-to-thickness ratios. As reported in [38], a 2 times larger span-to-thickness ratio was chosen to determine the bending modulus of Hylite with a thickness of 1.2 mm under a three-point bending condition, where the bending/elastic modulus ratio is approx. 1.34 inversely. However, the bending strength σ_b is greater than the tensile strength $UTS - ROM$, which is to be expected [39,40]. The ratio of the bending strength to direct tensile strength for all test series is approx. 2 based on the calculated values of each, as shown in the curves for σ_b and UTS in the figure. A clear relationship between them is preliminarily obtained; however, further influences, such as span-to-thickness ratios, may provide more insight into their relationship [41].

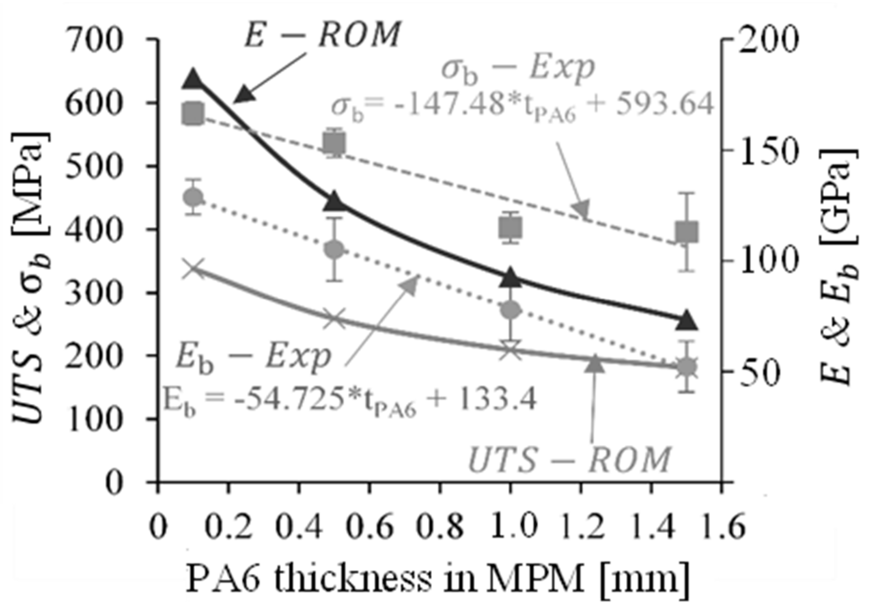

Figure 11. Relationship between the bending strength and bending modulus of the MPM and the core layer thicknesses at RT.

In Figure 12a, the major ε_1—minor ε_2 strains on the outer steel sheet (towards die rollers) after bending at RT are depicted for MPM with different core layer thicknesses. It can be observed that the maximum major strains in the press fins edge area are quite identical for MPMs with different core layer thicknesses (solid lines). In contrast, those in the punch edge region of three-point bending increase significantly with increasing core thickness [28]. This is due to the fact that the four-point bending method promises a constant bending between the press fins and the compressive stresses which occurred at the two centrally engaging press fins, which are lower in comparison to the three-point bending or V-bending method [19]. In addition, the strain distribution widens with increasing core thickness and support span, accompanied by smaller strain values between the press fins due to the compressive stress concentration occurring near the fins. Similarly, the minor strains (dashed lines) on the outer steel sheet of MPM increase with increasing core thickness and support width, as thicker core layers generate greater tensile stresses and more plastic deformation on the outer steel sheet [42]. More details about the strain distribution of the MPM samples at RT are illustrated in Figure 12b, in which the strain evolution is more visual for analysis. Clearly, at the edge of the sheet, the stress along the bend axis is zero at the free surface and plane strain does not exist, as marked with black arrows. It is usually observed that the edge of the sheet will curl as illustrated in Figure 12c. This happens because the stress state is approximately uniaxial tension near the edges of the sheet; the minor strain will be negative near the outer surface and positive near the inner surface, giving rise to the anticlastic curvature [43], which is accompanied by two orthogonal curvatures, R_x (i.e., longitudinal, x-direction) and R_y (transverse, y-direction) of opposite sign, shown in Figure 12d, having a significant effect on the spring-back behaviour [44].

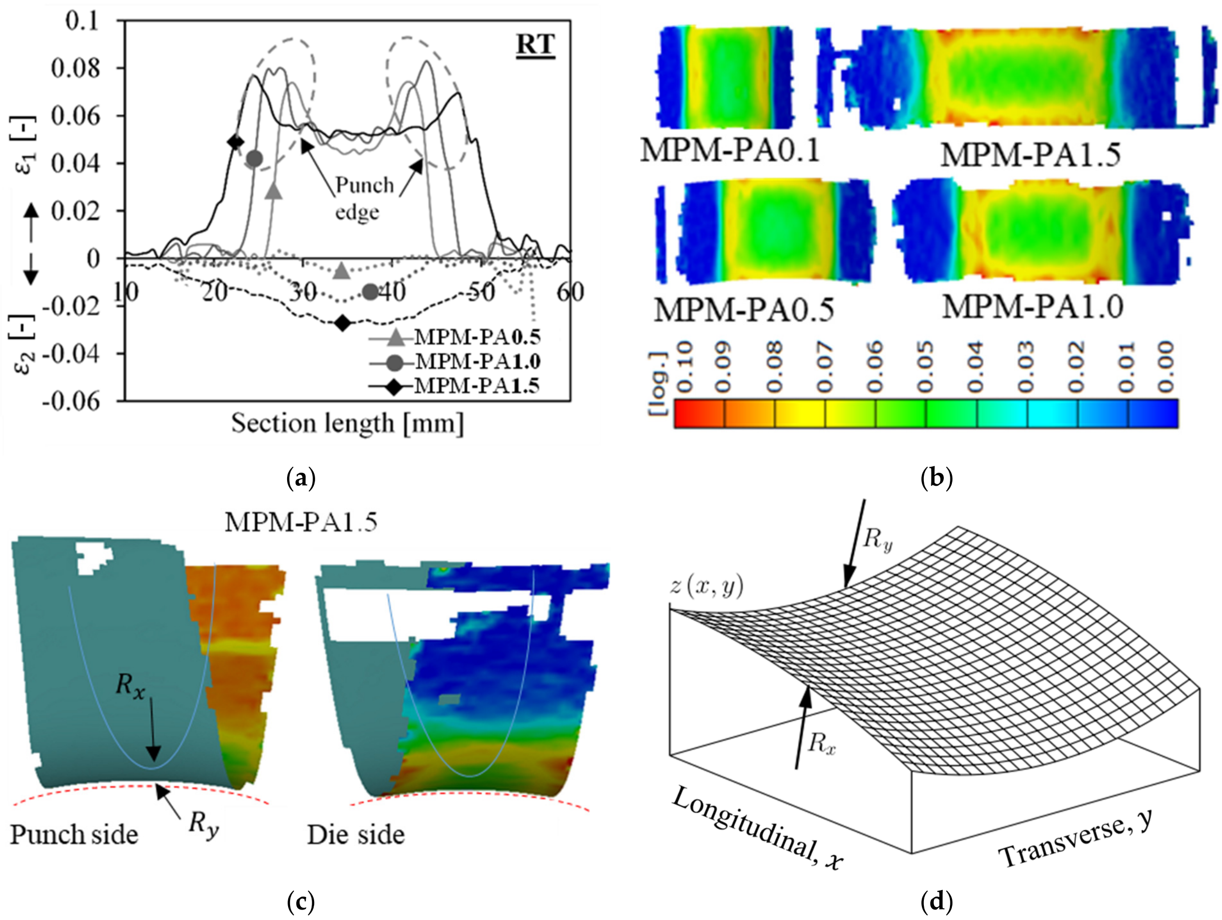

Figure 12. Strain evolution of the MPM after four-point bending test: (**a**) major and minor strains (die side) at RT with different core layer thicknesses, (**b**) DIC images: major strain (die side) evolution of MPM at RT, (**c**) anticlastic curvature of MPM-PA1.5 at RT, (**d**) illustration of typical anticlastic surface after bending [44].

3.2.3. Bending of the FML

Compared to MPM with a non-reinforced core, the bending forces of FML increase significantly with increasing core layer thickness and are greater than those of MPM due to the absolute higher stiffness of the organosheet compared to PA6. However, FML-RG1.0 and FML-RG2.0 showed significant failure at bending depths of approx. 8 and 10 mm, as evidenced by the decrease in bending force in Figure 13a. A sample image of FML-RG2.0 showing significant delamination is illustrated in the figure, while delamination in FML-RG1.0 is not evident, requiring further microscopic analysis in the next section. The reason for different degrees of delamination is that the thicker the core layer, the higher the interlaminar shear stress between the cover and core layers [45]. At RT, all samples showed localized strain evolution at the press fins region. In addition, plane strain deformation is observed with the minor strain along the axis of the bend close to zero in the sample middle, where the anticlastic curvature is less significant compared to MPM, as shown for FML-RG2.0 in Figure 13b. For narrow, initially flat sheets, the ratio between the longitudinal and the transverse curvatures is given by the Poisson ratio v, i.e., $R_y = R_x/v$ [44]. The difference between FML and MPM may be due to their different Poisson's ratios in the core, as a lower v of GF-PA6 would result in a larger R_y. And Poisson's ratio is decreased with increasing the fibre content [46]. However, the above-mentioned theory about the anticlastic curvature is based on a homogeneous material, not on hybrid materials.

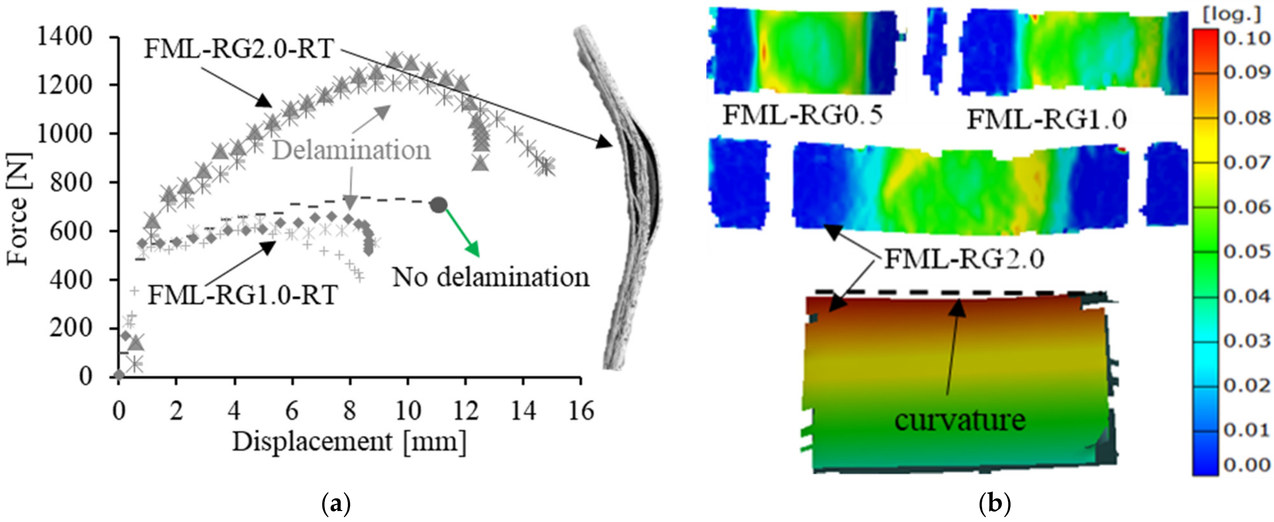

Figure 13. (**a**) Force evolution of FML with different core layer thicknesses under four-point bending conditions at RT, (**b**) DIC images: major strain (die side) evolution of FML at RT.

The effect of fibre volume fraction along the longitudinal direction of the FML sample on its bending force when using RGUD as a core layer is depicted in Figure 14. Since RGUD is stiffer in the warp direction than in the weft direction, the bending force of FML-RGUD^{X}1.0 is significantly higher than that of FML-RGUD^{Y}1.0. Also, the bending force of FML-RG1.0 is, as expected, located between that of FML-RGUD^X and FML-RGUD^Y. From the DIC images, it can be clearly seen that more stress concentration took place near the pressing fins for FML-RGUD^{Y}1.0 due to its lower stiffness in the transverse direction.

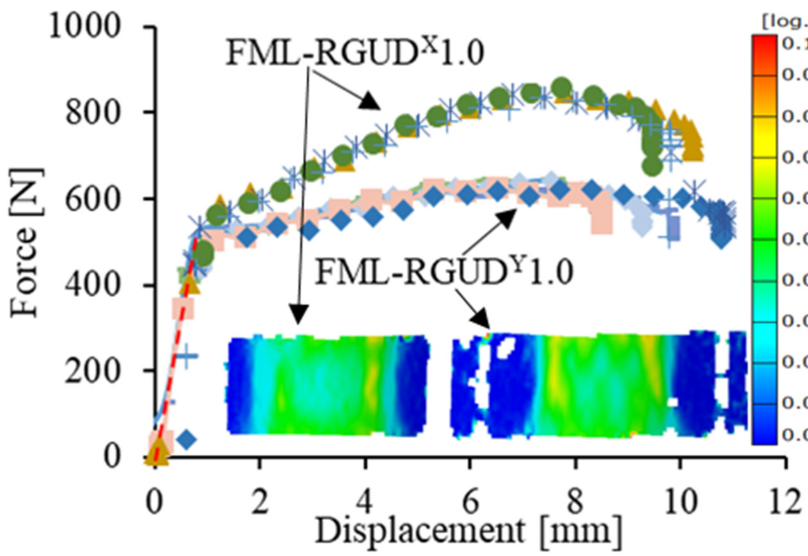

Figure 14. Force evolution of FML with organosheet RGUD under four-point bending conditions in transverse and longitudinal directions at RT and DIC images: major strain (die side).

Figure 15 shows the bending strength and modulus of FML. It can be accordingly stated that the bending properties of the sandwich materials are determined by the individual properties of their mono-materials and the bonding properties, too. At RT, the bending strengths of TS275 and RG were found to be approx. 594 ± 10 MPa and 561 ± 17 MPa in the previous bending experiments of MPM and RG. According to the ROM theory of the sandwich material, the bending strength of FML should decrease with the increase in core layer thickness. However, in the bending experiments, the bending strength of FML was found to be higher with increasing core layer thickness. This is similar to their tensile strength and elastic modulus, as shown in Figure 15a, where the dashed lines represent the measured bending strength and modulus, and the solid lines show the measured tensile strength and elastic modulus, respectively; and their values are calculated based on ROM. It can be seen that the $UTS - ROM$ for the FML decreases slightly with increasing core thickness. Due to the backing support effect of the steel cover sheet, the measured $UTS - Exp$ actually increases with increasing core thickness. Similar to $UTS - Exp$, the bending strength of FML increases with increasing core thickness. Furthermore, the bending strength of FML is higher than its tensile strength [47] and shows a linear relationship with the thickness of the core layer.

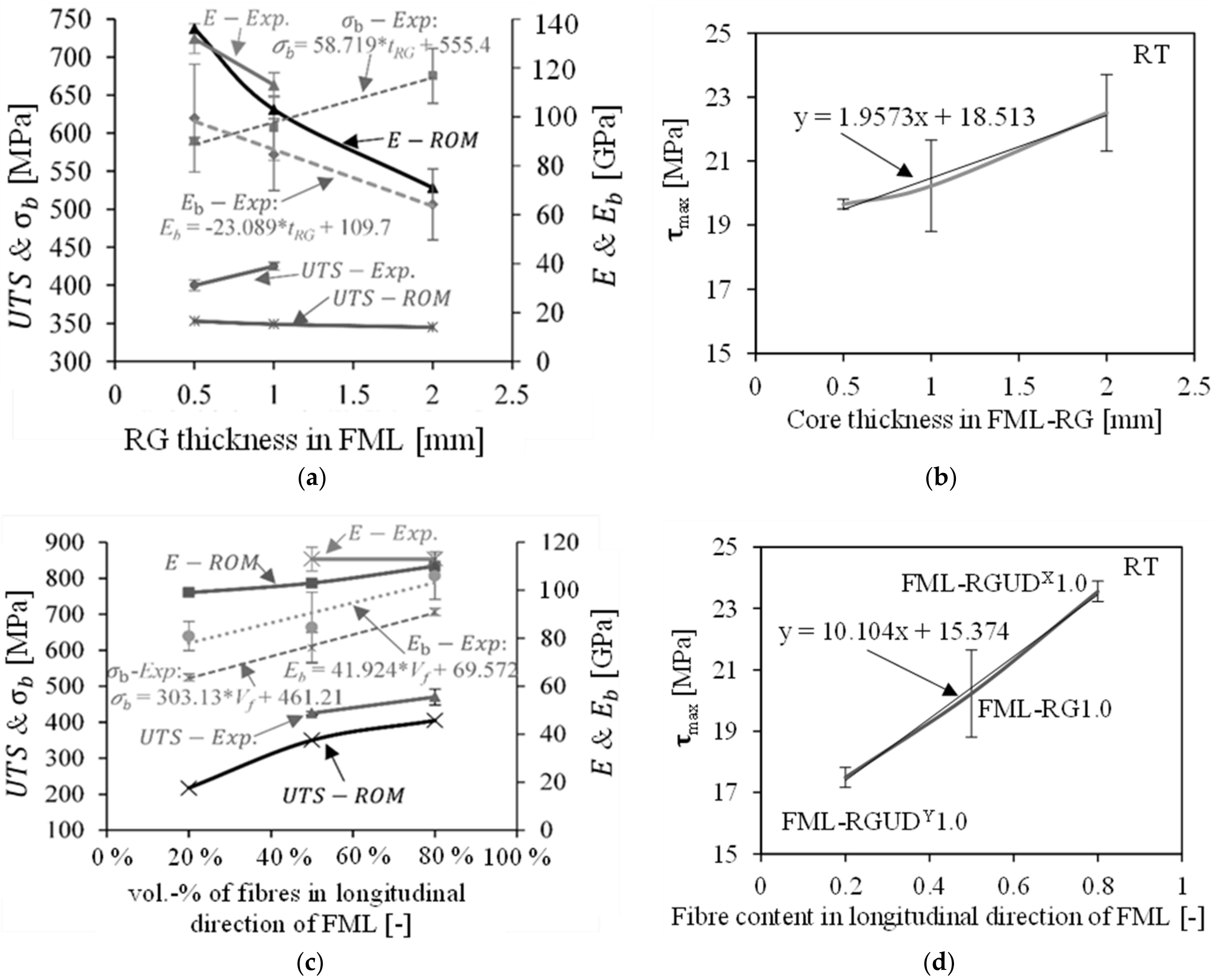

Figure 15. (**a**) Bending and tensile properties vs. core layer thickness, (**b**) maximum interlaminar shear strength vs. core layer thicknesses, (**c**) bending and tensile properties vs. fibre volume fraction in the longitudinal direction of the sample, (**d**) maximum interlaminar shear strength vs. fibre content in the longitudinal direction of the sample.

In addition, the bending modulus of FML also shows a linear relationship with core thickness and decreases significantly with increasing core thickness as the bending modulus of RG (21.5 ± 1.7 GPa) is significantly less than that of TS275 (133 ± 10 GPa). This is consistent with their elastic modulus, $E - Exp$ and $E - ROM$, which tends to decrease as the tensile modulus of RG is only 18 GPa, compared to 205 GPa for steel sheet TS275.

However, $E - Exp$ shows a tendency to be greater than the $E - ROM$ value as the volume fraction of the core layer increases, which is similar to the trend in its tensile strength, also due to the backing support effect of the steel cover sheet. The ratio of the bending strength to direct tensile strength for all test series of FML-RG samples is approx. 1.5, and that of the bending modulus to elastic modulus is 0.75, which is similar to that for MPM. Furthermore, in Figure 15b it can be seen that the interlaminar shear strength increases with increasing the core layer thickness, which is consistent with the findings of [45].

Changing the type of organosheet caused a difference in the fibre volume fraction in the longitudinal direction of the sample. At RT, both the bending strength and modulus showed an increasing trend with increasing fibre volume fraction, as seen in Figure 15c. The two dashed lines are the measured bending strength and modulus, the solid lines correspond to their $UTS - Exp$ and $UTS - ROM$, respectively. The tensile properties of the FML increase correspondingly with increasing fibre volume fraction in the tensile direction (longitudinal direction of the sample), similar to their bending properties. Similarly, the interlaminar shear strength increases with increasing fibre volume fraction in the longitudinal direction of the sample, see Figure 15d.

3.2.4. Failure Modes

Regarding the failure mode by delamination, FML-RGUD^{X}1.0 as an example can be seen in Figure 16a, indicating a microscopic delamination with a gap distance of less than 100 μm and a slight matrix fracture. The delaminated area is invisible without a microscope. The delamination occurs on the bottom side due to the maximum interlaminar shear stress caused by the bending process. However, no defects such as delamination are found in MPM due to the high interlaminar bond strength and lower stiffness of the core layer PA6, see Figure 16b.

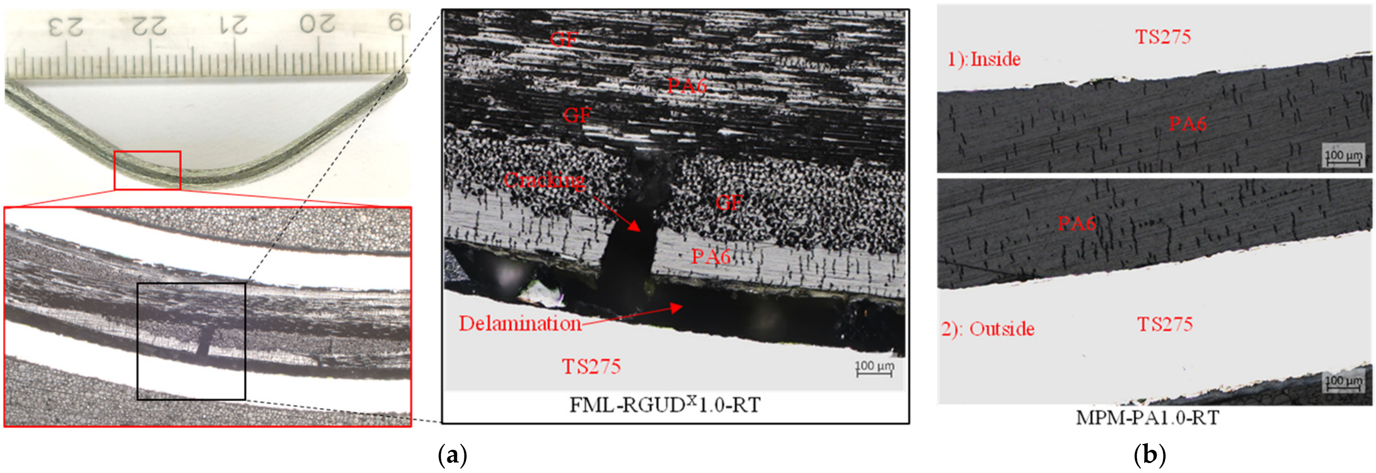

Figure 16. Micrographs of (**a**) FML-RGUD^{X}1.0-RT and (**b**) MPM-PA1.0-RT.

Another failure mode is the thickness changes. Figure 17 demonstrates the thickness deflection of the steel cover sheets (original thickness is about 0.4 mm) for different samples. Micrograph (1) shows the unique non-delaminated sample FML-RG1.0 marked with a green arrow in Figure 13a, in which the outer steel sheet is significantly thinner, while the inner steel sheet is thicker due to the large tensile/compressive stresses on the die/punch side of the sample, respectively. In contrast, FML samples with delamination and MPM samples showed no significant difference in the thickness of the steel cover sheets, see micrographs (2) and (3).

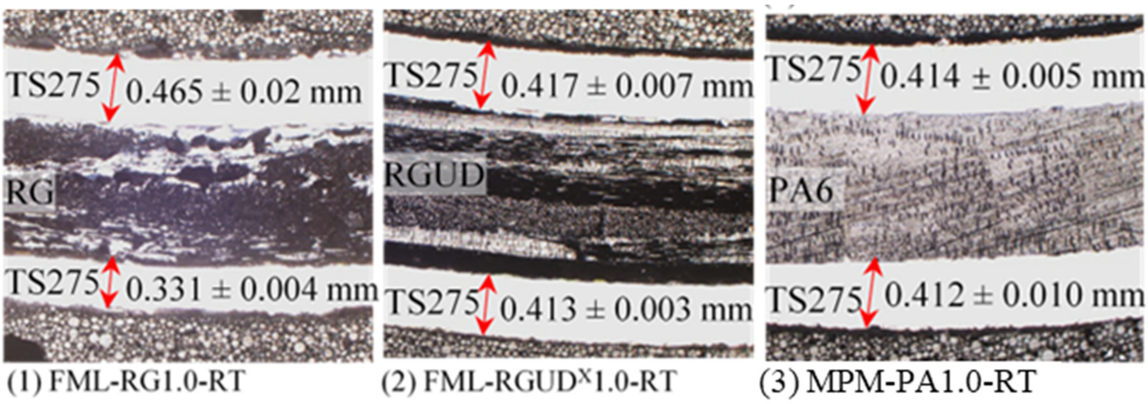

Figure 17. Thickness changes of the sandwich sample in steel cover sheets of MPM and FML.

3.3. Validation of the Analytical Model

The analytical calculation results were verified with the experimental ones for MPM and FML with different core layer thicknesses, see Figure 18a–d for MPM samples and Figure 18e–g for FML samples. It can be seen that the analytical results match well with experimental ones for MPM, despite the deviation of the analytical results of MPM-PA0.5 reaching about 10% in Figure 18b. For FML, the analytical values are in good agreement with the experimental ones for FML-RG0.5 in Figure 18e. However, high deviations of 20–25% were found for FML-RG1.0 and FML-RG2.0 with increasing loading path, although they were in good correlation at the beginning of plastic deformation, see Figure 18f,g. The reason is that the variable m of FML used to calculate the material parameters C_1 to C_4 in Equation (5) is hard to determine. In contrast to MPM and TS275, the tensile curve of FML is divided into two linearly increasing stages, see Figure 7c. In the second stage, the steel deforms plastically while the core layer remains elastic. And then, the core layer fractures while the tensile force drops steeply. Since the variable of m describes the plastic deformation of a homogeneous material, the variable of m is not available for the FML because of the non-homogeneity of the cover and core layers. Therefore, the value of m from TS275 was used in the calculation of the bending force of FML. As the core thickness in FML increases, the greater its role in the bending process, leading to a greater deviation between the analytical and experimental values.

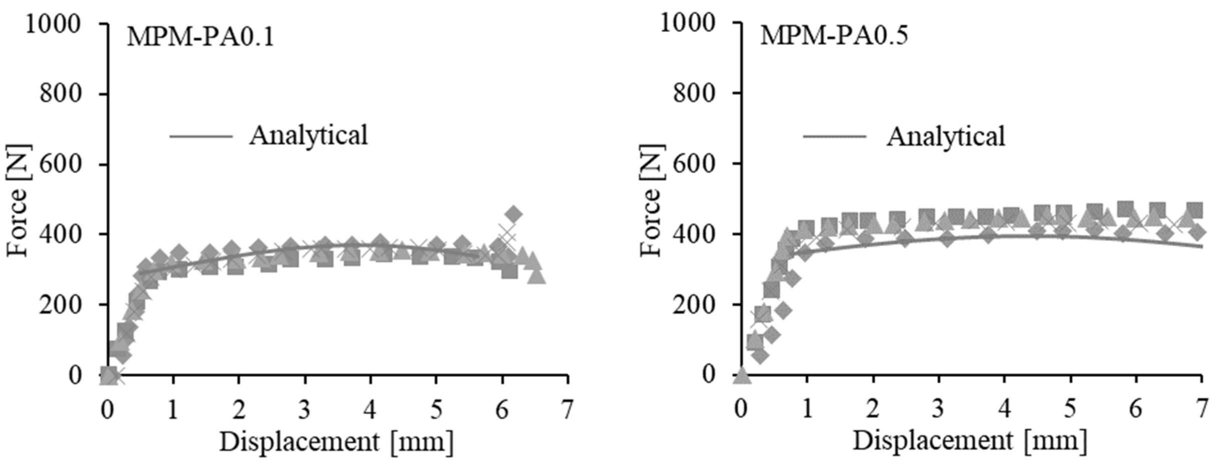

(**a**) (**b**)

Figure 18. *Cont.*

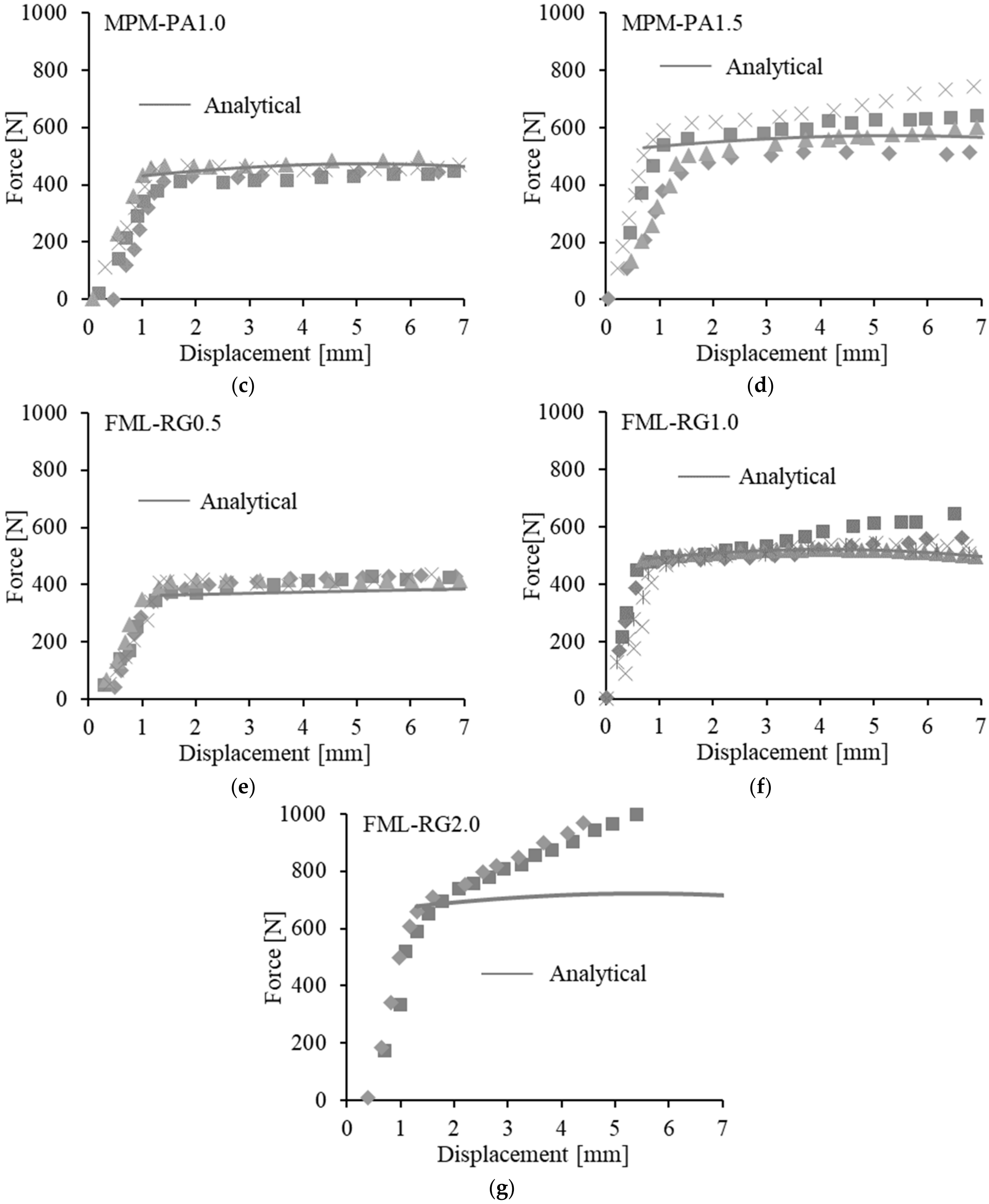

Figure 18. Validation of force evolutions for (**a**) MPM-PA0.1, (**b**) MPM-PA0.5, (**c**) MPM-PA1.0, (**d**) MPM-PA1.5, (**e**) FML-RG0.5, (**f**) FML-RG1.0 and (**g**) FML-RG2.0.

4. Conclusions and Outlook

In this paper, the mono-materials (cover sheet: TS275-0.4 mm and core layers: PA6, RG and RGUD) and their sandwich panels (MPM and FML) with different thickness combinations are used to characterize their tensile and bending properties. The relationship between the tensile and bending properties is described. Based on the obtained results, the following conclusions can be made:

- The tensile strength and elastic modulus of the MPM decrease with increasing thickness of the core layer PA6 due to its lower mechanical properties, corresponding to the ROM.
- The cover sheet supplies a backing support effect to the organosheet core layer, leading to a postponed fibre fracture. However, the sample fractures earlier with decreasing fibre volume fraction in the loading direction.
- For laminates under four-point bending conditions, the anticlastic curvature effect of MPM is much more significant than that of FML.
- For FML, the bending strength and interlaminar shear strength increase with increasing core layer thickness and the bending modulus decreases with increasing core layer thickness, which resembles its tensile mechanical properties.
- For both MPM and FML in this study, their bending and tensile properties have a definitive relationship with each other at different core layer thicknesses:
  - The bending moduli are smaller than the elastic moduli: a ratio of approx. 0.75;
  - The bending strengths are greater than the tensile strength: a ratio of approx. 2 for MPM and approx. 1.5 for FML.
- The analytical method achieves good agreement with the experimental ones for MPM. However, further modifications are necessary for FML.

Author Contributions: Conceptualization, W.H., M.H., G.Z. and H.P.; methodology, W.H. and M.H.; software, W.H.; validation, W.H.; investigation, W.H. and M.H.; resources, G.Z. and H.P.; data curation, W.H. and M.H.; writing—original draft preparation, W.H. and M.H.; writing—review and editing, M.H., G.Z., A.C. and H.P.; visualization, W.H.; supervision, G.Z., A.C. and H.P.; project administration, G.Z., A.C. and H.P.; funding acquisition, G.Z. and H.P. All authors have read and agreed to the published version of the manuscript.

Funding: This research was funded by the German Research Foundation, grant number 330043166.

Institutional Review Board Statement: Not applicable.

Informed Consent Statement: Not applicable.

Data Availability Statement: The authors are ready to share their research data upon request.

Acknowledgments: We would like to thank thyssenkrupp Steel Europe GmbH for their supplying the steel materials and SI Coatings GmbH for supplying the adhesion promoter.

Conflicts of Interest: The authors declare no conflict of interest.

List of Notations

Symbol	Term	Unit
α	Bending angle	[°]
ε_0	Yield strain	[-]
$\varepsilon_{\mathrm{pl}}$	Plastic strain	[-]
μ	Friction coefficient	[-]
σ_0	Yield stress	[MPa]
σ_{pl}	Plastic stress	[MPa]
σ_b	Bending strength	[MPa]
τ_{max}	Interlaminar shear strength	[MPa]
b	Sample width	[mm]
C_1, C_2, C_3, C_4	Material parameter	[-]
E	Elastic modulus	[GPa]
E_b	Bending modulus	[GPa]
F	Force	[N]
l_a	Distance between the contact points of the bent sheet with the punch & die	[mm]
L	Support width of the pressing fins	[mm]

m	Material parameter	[-]
s	Punch deflection	[mm]
t	Thickness of the sample	[mm]

References

1. Vogelesang, L.B.; Gunnink, J.W. ARALL: A materials challenge for the next generation of aircraft. *Mater. Des.* **1986**, *7*, 287–300. [CrossRef]
2. Rendigs, K.H. *Airbus and Current Aircrafts Metal Technologies*; Airbus: Bremen, Germany, 2008.
3. Wanhill, R.J.H. *Aerospace Materials and Material Technologies: GLARE®: A Versatile Fibre Metal Laminate (FML) Concept*; Springer: Singapore, 2017.
4. Asundi, A.; Choi, A. Fiber metal laminates: An advanced material for fiber metal laminates: An advanced material for future aircraft. *J. Mater. Process. Technol.* **1997**, *63*, 384–394. [CrossRef]
5. Reyes, G.; Cantwell, W.J. The mechanical properties of fibre-metal laminates based on glass fibre reinforced polypropylene. *Compos. Sci. Technol.* **2000**, *6*, 1085–1094. [CrossRef]
6. Reyes, G.; Kang, H. Mechanical behavior of lightweight thermoplastic fiber–metal laminates. *J. Mater. Process. Technol.* **2007**, *186*, 284–290. [CrossRef]
7. Paul, C.; Jaschinski, J. *Effiziente Mischbauweisen für Leichtbau-Karosserien: Abschlussbericht*; Wiedemann, S., Wessels, H., Wetterau, H.J., Eckstein, L., Schulte, T., Modler, N., Jaschinski, J., Eds.; Plattform FOREL, Institut für Leichtbau und Kunststofftechnik, TU Dresden: Dresden, Germany, 2016.
8. Scholz, P.; Schieck, F.; Müller, R.; Seidlitz, H.; Gerstenberger, C.; Osiecki, T.; Grbic, N.; Behrens, B.A.; Vucetic, M.; Neumann, A. Umformprozessketten für Bauteile aus Faser-Kunststoff/Metall-Verbunden. In Proceedings of the Europäische Forschungsgesellschaft für Blechverarbeitung (Kolloquium) 2015, BadBoll, Baden-Württemberg, Germany, 24–25 March 2015.
9. Tekkaya, A.; Hahn, M.; Hiegemann, L.; Weddeling, C.; Ben Khalifa, N. Umformen faserverstärkter thermoplastischer Kunststoff-Halbzeuge mit metallischen Deckblechen für den Leichtbau. In Proceedings of the Europäische Forschungsgesellschaft für Blechverarbeitung (Kolloquium) 2015, BadBoll, Baden-Württemberg, Germany, 24–25 March 2015.
10. Wielage, B.; Nestler, D.; Steger, H.; Kroll, L.; Tröltzsch, J.; Nendel, S. *CAPAAL and CAPET—New Materials of High-Strength, High-Stiff Hybrid Laminates: Integrated Systems, Design and Technology 2010*; Springer: Berlin/Heidelberg, Germany, 2011; ISBN 978-3-642-17384-4.
11. Springer Fachmedien Wiesbaden. Application potential of litecor in the body. *ATZextra Worldw.* **2014**, *19*, 108–111. [CrossRef]
12. Harhash, M.; Fischer, T.; Grubenmann, M.; Hua, W.; Heingärtner, J.; Hora, P.; Ziegmann, G.; Palkowski, H. Top-hat crashboxes of thermoplastic fibre-metal-laminates processed in one-step thermoforming: Experimental and numerical study. *Compos. B Eng.* **2021**, *226*, 109367. [CrossRef]
13. Chowdhury, M.A.; Hossain, S. A review on tensile and flexural properties of fiber-reinforced polymer composites. *J. Polym. Eng.* **2020**, *7*, 16–26.
14. Bae, J.M.; Kim, N.; Hattori, M.; Hasegawa, K.; Yoshinari, M.; Kawada, E.; Oda, Y. The flexural properties of fiber-reinforced composite with light-polymerized polymer matrix. *Int. J. Prosthodont.* **2001**, *14*, 33–39.
15. Ahmed, U.; Tariq, A.; Nawab, Y.; Shaker, K.; Khaliq, Z.; Umair, M. Comparison of mechanical behavior of biaxial, unidirectional and standard woven fabric reinforced composites. *Fibers Polym.* **2020**, *21*, 1308–1315. [CrossRef]
16. Baley, C.; Perrot, Y.; Busnel, F.; Guezenoc, H.; Davies, P. Transverse tensile behaviour of unidirectional plies reinforced with flax fibres. *Mater. Lett.* **2006**, *60*, 2984–2987. [CrossRef]
17. Cepeda-Jiménez, C.M.; Alderliesten, R.C.; Ruano, O.A.; Carreño, F. Damage tolerance assessment by bend and shear tests of two multilayer composites: Glass fibre reinforced metal laminate and aluminium roll-bonded laminate. *Compos. Sci. Technol.* **2009**, *69*, 343–348. [CrossRef]
18. Khalili, S.M.R.; Mittal, R.K.; Kalibar, S.G. A study of the mechanical properties of steel/aluminium/GRP laminates. *Mater. Sci. Eng.* **2005**, *412*, 137–140. [CrossRef]
19. Feraboli, P.; Kedward, K.T. Four-point bend interlaminar shear testing of uni- and multi-directional carbon/epoxy composite systems. *Compos. Part A Appl. Sci. Manuf.* **2003**, *34*, 1265–1271. [CrossRef]
20. Xie, M.; Adams, D.F. Study of three- and four-point shear testing of unidirectional composite materials. *Composites* **1995**, *26*, 653–659. [CrossRef]
21. Li, H.G.; Xu, Y.W.; Hua, X.G.; Liu, C.; Tao, J. Bending failure mechanism and flexural properties of GLARE laminates with different stacking sequences. *Compos. Struct.* **2018**, *187*, 354–363. [CrossRef]
22. Hua, W.; Fischer, T.; Harhash, M.; Ziegmann, G.; Palkowski, H. Study on processing galvanized steel/PA6 sandwich composites by hot-pressing: Influence of interface properties and surface treatment on the adhesion strength. *Compos. Struct.* **2020**, *236*, 111779. [CrossRef]
23. Hua, W. Forming Behaviour of Sandwich Materials Made of Steel Covers and Polyamide Cores with or Without Glass Fibre Reinforcements. Dissertation, Clausthal University of Technology, Clausthal-Zellerfeld, Germany, 2022.
24. Fischer, T. Entwicklung Einer Verbundoptimierten Prozessführung im Variothermen Pressverfahren. Dissertation, Clausthal University of Technology, Clausthal-Zellerfeld, Germany, 2022.

25. Deutsches Institut für Normung e. V. *Testing of Metallic Materials—Tensile Test Pieces: DIN 50125:2004-01*; Beuth Verlag GmbH: Berlin, Germany, 2009.
26. Deutsches Institut für Normung e. V. *Fibre-Reinforced Plastic Composites—Determination of Flexural Properties: DIN EN ISO 14125:1998-06*; Beuth Verlag GmbH: Berlin, Germany, 2011.
27. Bellini, C.; Di Cocco, V.; Iacoviello, F.; Sorrentino, L. Performance evaluation of CFRP/Al fibre metal laminates with different structural characteristics. *Compos. Struct.* **2019**, *225*, 111117. [CrossRef]
28. Harhash, M.; Gilbert, R.R.; Hartmann, S.; Palkowski, H. Experimental characterization, analytical and numerical investigations of metal/polymer/metal sandwich composites—Part 2: Free bending. *Compos. Struct.* **2019**, *232*, 111421. [CrossRef]
29. Kreulitsch, H. *Formgebung von Blechen und Bändern durch Biegen*; Springer: Wien, Austria, 1995; ISBN 3-211-82595-9.
30. Botelhoa, E.C.; Silva, R.A.; Pardini, L.C.; Rezende, M.C. A review on the development and properties of continuous fiber/epoxy/aluminum hybrid composites for aircraft structures. *Mater. Res.* **2006**, *9*, 247–256. [CrossRef]
31. Bellini, C.; Di Cocco, V.; Iacoviello, F.; Sorrentino, L. Experimental analysis of aluminium/carbon epoxy hybrid laminates under flexural load. *Frat. Integrita Strutt.* **2019**, *13*, 739–747. [CrossRef]
32. Wu, X.; Pan, Y.C.; Wu, G.Q.; Huang, Z.; Tian, R.; Sun, S.Q. Flexural behaviour of CFRP/MG hybrid laminates with different layers thickness. *Adv. Compos. Lett.* **2017**, *26*, 168–172. [CrossRef]
33. Schirmaier, F.J.; Weidenmann, K.A.; Kärger, L.; Henning, F. Characterisation of the draping behaviour of unidirectional non-crimp fabrics (UD-NCF). *Compos. Part A Appl. Sci. Manuf.* **2016**, *80*, 28–38. [CrossRef]
34. Galkin, S.; Kunze, E.; Kärger, L.; Böhm, R.; Gude, M. Experimental and numerical determination of the local fiber volume content of unidirectional non-crimp fabrics with forming effects. *J. Compos. Sci.* **2019**, *3*, 19. [CrossRef]
35. LANXESS Deutschland GmbH. *Tepex Materials Data Sheet: Tepex®dynalite 102-RG600(x)/47%*; LANXESS Deutschland GmbH: Köln, Germany, 2014.
36. Tan, Y.L.; Huang, C.H.; Guo, Z.X.; Yu, J. Morphology and mechanical properties of polyamide 6/polystyrene blends prepared by diffusion and subsequent polymerization of styrene in polyamide 6 pellets. *Materials* **2018**, *11*, 776. [CrossRef]
37. Wang, C.L.; Zheng, S.L.; Wang, H.F. Evaluation of mechanical properties of polyamide 6(PA6) filled with wollastonite and inorganic modified wollastonite. *Appl. Mech. Mater.* **2012**, *217–219*, 522–525. [CrossRef]
38. Hufenbach, W.; Jaschinski, T.; Weber, T.; Weck, D. Numerical and experimental investigations on HYLITE sandwich sheets as an alternative sheet metal. *Arch. Civ. Mech.* **2008**, *8*, 67–80. [CrossRef]
39. Yekani Farda, M.; Raji, B.; Chattopadhyay, A. The ratio of flexural strength to uniaxial tensile strength in bulk epoxy resin polymeric materials. *Polym. Test.* **2014**, *40*, 156–162. [CrossRef]
40. Whitney, J.M.; Knight, M. The relationship between tensile strength and flexure strength in fiber-reinforced composites. *Exp. Mech.* **1980**, *20*, 211–216. [CrossRef]
41. Kim, D.J.; Naaman, A.E.; Tawil, E.I. Correlation between tensile and bending behavior of FRC composites with scale effect: High Performance, Fiber Reinforced Concrete, Special Loadings and Structural Applications. In Proceedings of the Fracture Mechanics of Concrete and Concrete Structures, Jeju, Republic of Korea, 23–28 May 2010.
42. Parsa, M.H.; Mohammadi, S.V.; Aghchai, A.J. Al3105/polypropylene/Al3105 laminates springback in V-die bending. *Int. J. Adv. Manuf. Technol.* **2014**, *75*, 849–860. [CrossRef]
43. Horrocks, D.; Johnson, W. On anticlastic curvature with special reference to plastic bending: A literature survey and some experimental investigations. *Int. J. Mech. Sci.* **1967**, *9*, 835–861. [CrossRef]
44. Wang, J.F.; Wagoner, R.H.; Matlock, D.K.; Barlat, F. Anticlastic curvature in draw-bend springback. *Int. J. Solids Struct.* **2005**, *42*, 1287–1307. [CrossRef]
45. Kuhtz, M.; Buschner, N.; Henseler, T.; Hornig, A.; Klaerner, M.; Ullmann, M.; Jäger, H.; Kroll, L.; Kawalla, R. An experimental study on the bending response of multi-layered fibre-metal-laminates. *J. Compos. Mater.* **2019**, *53*, 2579–2591. [CrossRef]
46. Illing, T.; Gotzig, H.; Schoßig, M.; Bierögel, C.; Grellmann, W. Influence of hygrothermal aging on poisson's ratio of thin injection-molded short glass fiber-reinforced PA6. *Fibres* **2016**, *4*, 17. [CrossRef]
47. Rajkumar, G.R.; Krishna, M.; Narasimhamurthy, H.N.; Keshavamurthy, Y.C.; Nataraj, J. Investigation of tensile and bending behavior of aluminum based hybrid fiber metal laminates. In Proceedings of the International Conference on Advances in Manufacturing and Materials Engineering, Mangalore, Karnataka, India, 27–29 March 2014.